JOURNAL OF GEOPHYSICAL RESEARCH, VOL. 102, NO. D9, PAGES 10,739–10,750, MAY 20, 1997

In situ observations of air traffic emission signatures in the North Atlantic flight corridor

H. Schlager,[1] P. Konopka,[1] P. Schulte,[1] U. Schumann,[1] H. Ziereis,[1] F. Arnold,[2]
M. Klemm,[2] D.E. Hagen,[3] P.D. Whitefield,[3] and J. Ovarlez[4]

Abstract. Focussed aircraft measurements have been carried out over the eastern North Atlantic to search for signals of air traffic emissions in the flight corridor region. Observations include NO, NO_2, HNO_3, SO_2, O_3, H_2O, total condensation nuclei (CN), and meteorological parameters. A flight pattern with constant-altitude north-south legs across the major North Atlantic air traffic tracks was flown. Signatures of air traffic emissions were clearly detected for NO_x, SO_2, and CN with peak concentrations of 2 ppbv, 0.25 ppbv, and 500 cm^{-3}, respectively, exceeding background values by factors of 30 (NO_x), 5 (SO_2), and 3 (CN). The observed NO_x, SO_2, and CN peaks were attributed to aircraft plumes based on radar observations of the source air traffic and wind measurements. Major aircraft exhaust signatures are due to relatively fresh emissions, i.e., superpositions of 2 to 5 plumes with ages of about 15 min to 3 hs. The observed plume peak concentrations of NO_x compare fairly well with concentrations computed with a Gaussian plume model using horizontal and vertical diffusivities as obtained by recent large-eddy simulations, measured vertical wind shear, and the corridor air traffic information. For the major emission signatures a mean CN/NO_x abundance ratio of 300 $cm^{-3}ppbv^{-1}$ was measured corresponding to an emission index (EI) of about 10^{16} particles per 1 kg fuel burnt. This is higher than the expected soot particle EI of modern wide-bodied aircraft. For the most prominent plumes no increase of HNO_3 concentrations exceeding variations of background values was observed. This indicates that only a small fraction of the emitted NO_x is oxidized in the plumes within a timescale of about 3 hs for the conditions of the measurements.

1. Introduction

Emissions from air traffic in heavily used corridors may cause perturbations of the composition and radiative properties of the upper troposphere and lower stratosphere [e.g., *Schumann*, 1994; *WMO*, 1995]. Jet engine exhaust that may alter the ambient atmosphere includes, among other components, nitrogen oxides (NO_x = NO + NO_2), sulfur-containing species, and soot. Emitted NO_x leads to formation of ozone (O_3) at altitudes around the tropopause [*Johnson et al.*, 1992; *Beck et al.*, 1992; *Brasseur et al.*, 1996]. Because of nonlinear chemistry the O_3 formation efficiency from additional NO_x input is dependent on the existing NO_x abundance level [*Ehhalt and Rohrer*, 1995] and thus also on the dispersion and mixing processes of highly concentrated exhaust plumes in the corridors. Part of the sulfur in aviation fuel is oxidized to sulfuric acid in the engine and exhaust jet which in turn nucleates with water vapor, generating additional aerosols [*Reiner and Arnold*, 1993, 1994; *Miake-Lye et al.*, 1994; *Frenzel and Arnold*, 1994; *Kärcher et al.*, 1995; *Zhao and Turco*, 1995]. Emitted soot particles may be partly activated in the exhaust plume to cloud condensation nuclei (CN), which influence the formation and radiative properties of clouds [*Schumann et al.*, 1996].

Emissions from individual jet aircraft at cruise altitude have been measured for subsonic [*Arnold et al.*, 1992; *Fahey et al.*, 1995b; *Schulte and Schlager*, 1996; *Schumann et al.*, 1996; *Whitefield et al.*, 1996] and supersonic [*Fahey et al.*, 1995a] aircraft. However, it has been difficult to detect aircraft emission signatures in air traffic corridors. Numerical simulations using a Gaussian plume model predict a very inhomogeneous ("spotty") concentration field in a major flight corridor due to air traffic emissions [*Schumann and Konopka*, 1994]. In airborne measurements within the North Atlantic flight corridor at times and regions with relatively little traffic a few NO plumes from aircraft have been detected [*Schlager et al.*, 1994] and analyzed with re-

[1]Institut für Physik der Atmosphäre, Deutsche Forschungsanstalt für Luft- und Raumfahrt, Oberpfaffenhofen, Germany.
[2]Bereich Atmosphärenphysik, Max-Planck-Institut für Kernphysik, Heidelberg, Germany.
[3]Laboratory for Cloud and Aerosol Sciences, University of Missouri at Rolla.
[4]Laboratoire de Météorologie Dynamique, Ecole Polytechnique, Palaiseau, France.

Paper number 96JD03748.
0148-0227/97/96JD-03748$09.00

spect to lateral and vertical spreading for timescales from 5 to 90 min [*Schumann et al.*, 1995]. An analysis of DC-8 data obtained during the second Airborne Arctic Stratospheric Expedition has revealed a few NO_y (total reactive nitrogen) spikes that were attributed to air traffic plumes based on corresponding CO_2 spikes [*Zheng et al.*, 1994].

In this study we investigate signatures of aircraft emissions (NO_x and SO_2, particles) above ambient background concentrations resulting from peak traffic conditions in the North Atlantic flight corridor. In November 1994, research flights were made over the eastern North Atlantic as part of the Pollution From Aircraft Emissions in the North Atlantic Flight Corridor (POLINAT) project. Here observations of one mission are reported where the research aircraft was flying perpendicular to the major corridor tracks during the main eastbound traffic flow. The measured NO_x concentration field is compared with simulations obtained with a plume dispersion model using collected air traffic data and wind measurements.

2. Measurement Details

The Deutsche Forschungsanstalt für Luft- und Raumfahrt (DLR) "Falcon" research aircraft was used as sampling platform. This twin-engine jet aircraft has a cruise airspeed of about 180 ms^{-1}. It reaches well the typical cruising flight levels used by airliners crossing the North Atlantic. Falcon measurements to be reported in this study were performed on November 6, 1994, between 0730 and 0900 UTC based from Shannon Airport, Ireland.

2.1. Sampling Strategy

The measuring day was selected on the basis of forecasted back trajectories ending in the measuring area and other meteorological informations which indicate that air traffic signatures will not be masked by strong variations of trace gas abundances due to fast vertical transport of polluted air from the boundary layer or lightning. To obtain most pronounced air traffic signals, a measuring area was chosen where the major air traffic routes of the organized North Atlantic track system has been fixed for November 6, 1994, (between 50°and 54°N), and a measuring time close to the predicted peak eastbound traffic flow.

The flight pattern included three north-south crossings of the main traffic tracks, all along 12°W at the most frequently used flight level for eastbound air traffic (37,000 feet, about 11.3 km). The Falcon operated under radar control within the Shannon air traffic control area for safety reasons. Beginning 2 hours prior to the measuring flight and continuing during the measurements, information on the air traffic passing the Falcon legs were recorded from the radar observations at the Air Traffic Control Center of Shannon, including the aircraft movements between 6°W and 15°W, cruising

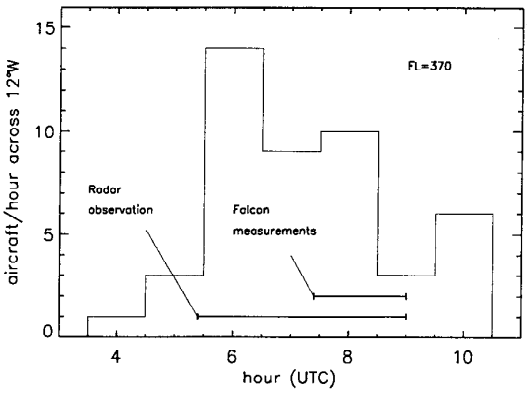

Figure 1. Flow of eastbound traffic across the north-south measuring track along 12°W at flight level 37,000 feet (11.3 km) and time periods of radar recordings and airborne observations.

levels, aircraft types, and actual Mach numbers. In addition, the complete data of air traffic operating in the radio-controlled Shanwick Oceanic Area between 15°W and 30°W were collected for the entire measuring day.

Figure 1 shows the traffic flow across the measuring track at 37,000 feet and 12°W during the eastbound traffic hours on November 6, 1994, between 50°and 54°N. Also indicated are the time periods of radar observations and Falcon measurements. For comparison, the total eastbound traffic before the end of Falcon measurements includes 43 and 198 aircraft at 37,000 feet and at all corridor flight levels, respectively. Thus the radar records cover nearly the complete air traffic at 37,000 feet before and during the measuring flight.

2.2. Instrumentation

Simultaneous measurements of NO, NO_2, O_3, H_2O, HNO_3, SO_2, CN, and meteorological parameters were performed from the Falcon for this study.

The NO and NO_2 instruments, operated by DLR, use conventional NO/O_3 chemiluminescence technique including a zero volume upstream of the reaction vessel [*Fontijin et al.*, 1970; *Ridley and Howlett*, 1974; *Kley and McFarland*, 1980]. Sampling for the NO_x detectors was made through a single Teflon tube from outside the aircraft boundary layer. In the aircraft cabin the sample air was split into NO and NO_2 channels at a constant pressure of 80 hPa independent of the aircraft measuring altitude by pumping excess sample air through a pressure-controlled valve. In the NO_2 channel the air sample was irradiated with broadband UV light (320–400 nm) using a 500-W high-pressure Xenon arc lamp for partial photodissociation of NO_2 to NO [*Kley and McFarland*, 1980]. The sample air mass flow was kept constant at 3 L min^{-1} (STP) for each instrument channel. The photolysis chamber was Peltier-cooled to keep its temperature below 15°C for minimizing thermal dis-

sociation of other reactive nitrogen species. To obtain a high spatial resolution of the measurements, a short sample air residence time in the photolysis chamber of 2 s was chosen, taking into account a photolytic efficiency of only 0.35.

During the flight, both chemiluminescent detectors were operated in modes for measure, zero, and calibrate (sensitivity and baseline determination). In addition, preflight and postflight calibrations included checks of the photolytic efficiency using NO_2 calibration air generated from a NO standard by titration with O_3. The overall uncertainty of NO measurements is 10% and 20% for concentration levels of about 1.0 ppbv and 0.1 ppbv, respectively. The accuracy of the NO_2 measurements is 30% and 50% for levels of about 1.0 ppbv and 0.2 ppbv, respectively, and NO_2/NO ratios around 1.

Ozone was measured using an UV absorption photometer operated by DLR. In this probe, sample air is passed through an absorption chamber (cell length, 300 mm; inner diameter, 5 mm) that is irradiated by a temperature-controlled mercury lamp. Detection of the transmitted light is made by a silicon photodiode. After each 1-s interval the sample air is periodically scrubbed of ozone. Thereby the instrument cycled through a reference and measuring mode with a time resolution of 2 s. The instrument pump was operated at a constant pumping speed of about 3 L min^{-1} (STP). The sensitivity of the instrument was checked before and after each flight using ground-based ozone standards. The accuracy of the instrument is 5% or 3 ppbv, depending on which value is larger.

Water vapor was measured by a frost-point hygrometer built and operated by the Laboratoire de Météorologie Dynamique (LMD) [*Ovarlez*, 1991; *Ovarlez and Ovarlez*, 1994]. With this instrument the onset of water vapor sublimation on a metal mirror is detected optically. The mirror temperature is controlled using cryogenic cooling. The accuracy of the determination of H_2O volume mixing ratios is 5%.

HNO_3 and SO_2 were continuously measured using a chemical ionization mass spectrometer developed and operated by the Max-Planck-Institut für Kernphysik (MPI-K) [*Arnold and Hauck*, 1985; *Arnold and Knop*, 1987; *Möhler et al.*, 1993]. In this measuring system, ambient air is sampled through an ion–flow tube reactor into which are injected reactant ions formed in an ion source. Determination of gaseous HNO_3 and SO_2 builds on selective ion-molecule reactions with known rate coefficients and requires the measurement of the corresponding production and reaction ratio with the mass spectrometer and the ions residence time in the flow tube. A cryogenically pumped (liquid neon) quadrupole mass spectrometer is used for ion mass analysis. Precision and accuracy of the technique are 20% and 40%, respectively.

Total condensation nuclei were measured with a CN counter that is part of the Mobile Aerosol Sampling System (MASS) of the University of Missouri-Rolla (UMR) [*Hagen et al.*, 1993; *Whitefield and Hagen*, 1995]. Volatile and nonvolatile particles were sampled through an unheated inlet line and exposed to a supersaturated butanol vapor which condenses on the particles, leading to sizes that can be optically detected. Particles in the diameter range from about 7 nm to 1.0 μm were counted. The latter limit is due to particle loss by impaction on walls of the inlet line. Precision and accuracy of the instrument are 10% and 20%, respectively.

Meteorological data were provided by DLR. Temperature was measured on board the Falcon using Rosemount Pt100 and Pt500 probes with an accuracy of 0.5 K. Static pressure was measured using a Rosemount 1201F1 transducer with an accuracy of 1 hPa. Wind was determined with a five-hole probe at the tip of a nose boom and an inertial navigation system with an accuracy of 1.5 ms^{-1} for the horizontal wind [*Bögel and Baumann*, 1991].

3. Experimental Results

3.1. Corridor Observations

Figure 2 shows time series of various measured parameters at three successive constant-altitude legs (A, B, and C) made at 11.3 km along 12°W while the Falcon was flying back and forth, from north to south, perpendicular to the main flight corridor. The observations were made between 073940 and 091319 UTC (27,580 s and 33,199 s). The time of sunrise is also marked in Figure 2. The measuring altitude was near the tropopause. The southern part of the flight legs was within the troposphere, the northern part within the stratosphere. This can be clearly seen from the measured horizontal distribution of the O_3, H_2O, and HNO_3 mixing ratios. The relative humidity with respect to ice did not exceed 70%, in agreement with the fact that no persistent contrails were observed. The wind came mainly from westerly directions, with wind speed varying between about 30 ms^{-1} at the northern part and near zero at the southern part of the flight legs. Figure 2 presents 5-s data for NO, NO_c (=NO + 0.35 NO_2), and CN; 10-s data for O_3 and H_2O; 12-s data for HNO_3 and SO_2; and 1-s data for the meteorological parameters.

Simultaneous sharp spikes in NO and NO_c concentrations were observed along all measuring legs with peak mixing ratios up to 1.3 ppbv for the integration time used. In between, low background mixing ratios were found (50 pptv for NO). Note that the peak concentrations in short-range spikes are smaller for NO_c compared to NO. This is due to the longer residence time of the sample air in the NO_c channel including the photolysis cell. Determination of NO_2 from short-term varying NO and NO_c data requires peak integration. The time spans of the sharp NO and NO_c variations range from 8 s to 32 s, corresponding to horizontal distances of 1.5 km to 5.5 km.

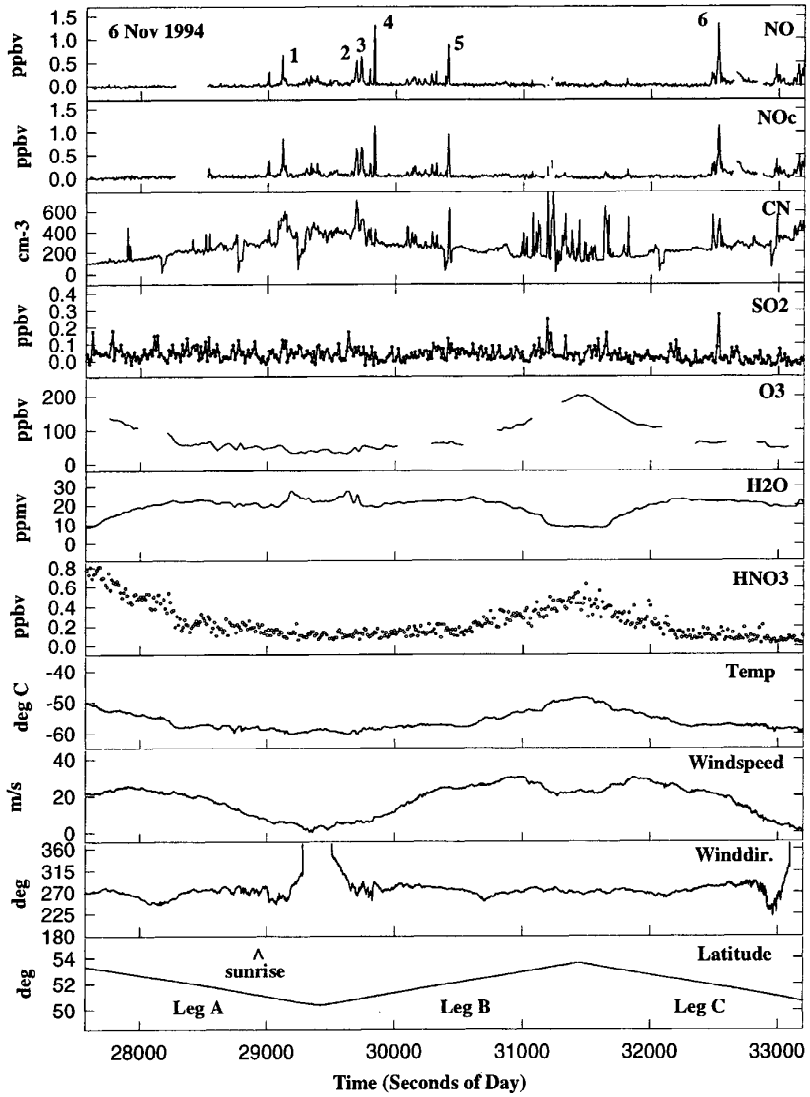

Figure 2. Time series for NO, NO_c (=NO + 0.35 NO_2), CN, SO_2, O_3, H_2O, HNO_3, temperature, wind speed, wind direction, and latitude measured on November 6, 1994, during crossings of the major air traffic tracks in the North Atlantic flight corridor. Observations were made along north-south oriented flight legs at constant longitude of 12°W and constant pressure altitude of 37,000 feet (11.3 km). Note that peak concentrations in NO_c spikes are more strongly attenuated than those in NO spikes owing to a longer residence time of the sample air in the NO_2 instrument.

Coincident sharp increases of CN concentrations were found for many NO and NO_c spikes. For one major NO and NO_c peak, a simultaneous SO_2 peak was clearly detected. Corresponding small-scale variations for O_3 and H_2O, which should occur if the NO, NO_c, SO_2, and CN peaks are due to small-scale displacements of constant mixing ratio surfaces relative to the flight legs at constant pressure altitude were not observed. This indicates fresh NO_x, SO_2 and CN emissions.

In the stratospheric part of leg B and leg C between about 31,000 s and 32,000 s, strong small-scale variations of CN number densities were observed which are in most cases not correlated with corresponding NO and NO_c variations. These CN variations might be due to a layered structure of the CN distribution which is occasionally observed in the lowermost stratosphere [e.g., *Wilson et al.*, 1991].

3.2. Attribution of Spikes to Air Traffic

In order to trace the observed coincident NO, NO_c, SO_2, and CN peaks back to air traffic emissions, the ex-

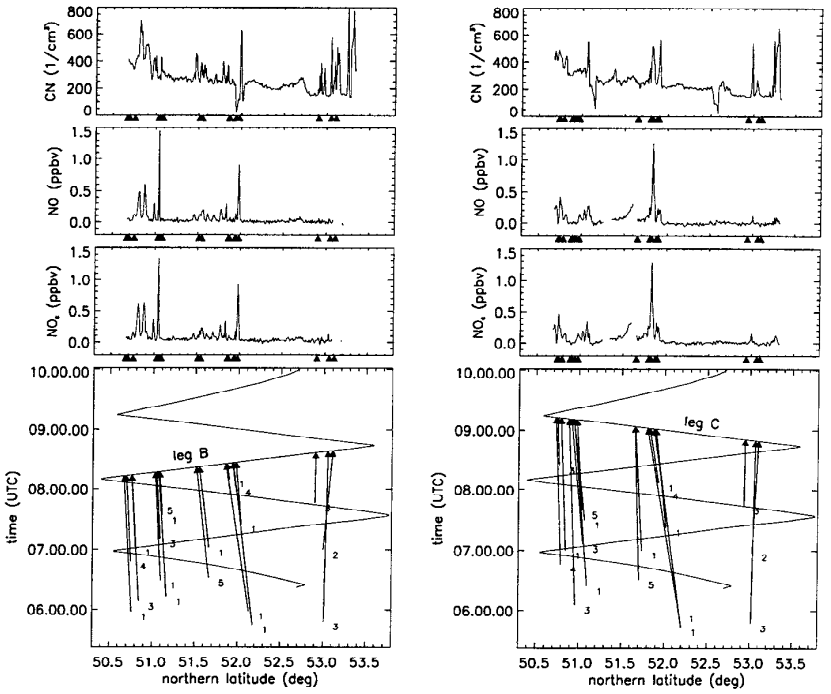

Figure 3. Observed CN, NO, and NO_c distribution on November 6, 1994, along (left) S-N measuring leg B and (right) N-S leg C shown in Figure 2 together with calculated plume air parcel trajectories ending at predicted Falcon intersection positions. The arrows are labeled with numbers indicating the source aircraft type (1; B-747, 2; B-757, 3; B-767, 4; EA-31, 5; MD-11).

pected positions of aged aircraft exhaust plumes along the Falcon track were determined from the collected air traffic data and the wind measurements aboard the Falcon. The advection of the individual plumes was calculated using a constant horizontal wind direction and speed as measured at the crossing point of the Falcon with the source aircraft tracks along 12°W (see appendix). The Falcon wind data were smoothed by 30-s averaging for this purpose.

The predicted plume intersection points for the measuring legs B and C across the flight corridor are shown in Figure 3. The bottom panel depicts the track of the Falcon in north-south direction versus time along constant latitude and altitude of 12°W and 11.3 km, respectively. The arrows show the trajectories of exhaust plume air parcels which should be intersected by the Falcon at the positions of the arrowheads along leg B (flight direction S-N) and leg C (flight direction N-S). Differences in the positions of the arrowheads and tail ends correspond to the latitudinal displacements and ages of the plume air parcel, respectively. Displacements in north-south direction are moderate owing to prevailing westerly winds. The arrows are labeled with numbers indicating the source aircraft type (1; B-747, 2; B-757, 3; B-767, 4; EA-31, 5; MD-11). The top three panels in Figure 3 show the measured NO_c, NO, and CN concentrations along leg B and leg C.

The predicted plume intersection positions along the two successive Falcon legs across the flight corridor correspond fairly well to the positions of the observed NO_c, NO and CN peaks within the uncertainty for the calculated plume positions. The accuracy of the assumed mean horizontal wind speed is $\pm 5\ m\,s^{-1}$, resulting in an uncertainty for the predicted plume position of about $\pm 0.25°$with respect to latitude for a plume travel time of 2 hours. The comparison reveals that in most cases, measured peaks are due to superpositions of several aircraft plumes having ages between about 15 min and 3 hours.

3.3. Abundance Ratio of Emission Species in Plumes

The partitioning of NO_2 and NO observed in the multiple plumes was examined for the most prominent peaks, labeled 1 through 6 in Figure 2. Details on the measurements in these plumes are given in Table 1.

The NO_2/NO ratios in the individual plumes were determined from the NO_c and NO integrals above background values in the spikes and the measured efficiency of the photolysis system ($f = 0.35$) during the preflight and postflight calibrations. The NO_2/NO obtained are also listed in Table 1.

In Figure 4 these values are compared with calculated NO_2/NO ratios assuming a photochemical steady

Table 1. Observations in Major Plumes

	Plume					
	1	2	3	4	5	6
Time, UTC	080515	081452	081528	081713	082648	090208
Latitude, °W	50.85	50.81	50.87	51.04	51.97	51.83
Longitude, °N	12.0	12.0	12.0	12.0	12.0	12.0
p, hPa	217.0	217.5	217.0	217.5	217.3	217.4
T, K	213.9	213.9	213.9	214.4	215.5	215.5
ΔNO, ppbvs	4.0	10.7	10.0	8.9	9.7	19.4
$\Delta NO_2/\Delta NO$, ppbv ppbv^{-1}	1.65	0.635	0.56	0.245	0.48	0.2
ΔNO_x, ppbvs	10.6	17.5	15.6	11.1	14.4	23.3
ΔCN, cm^{-3}s		5300	5880		6252	5342
ΔSO_2, ppbvs						4.1
$\Delta CN/\Delta NO_x$, cm^{-3}ppbv^{-1}		301	375		434	229
$\Delta SO_2/\Delta NO_x$ ppbv ppbv^{-1}						0.13

Blank entries denote cases where plume concentrations are not clearly distinguishable from background variations. Δ denotes the peak integral of the associated emission species.

state between daytime NO_2 and NO according to

$$\frac{[NO_2]}{[NO]} = \frac{k[O_3]}{j_{NO_2}} \quad (1)$$

where brackets denote concentrations, k is the temperature-dependent reaction rate constant of O_3 with NO, and j_{NO_2} is the photodissociation coefficient for NO_2. The concentration of O_3 is taken from the measurements, k is from *Atkinson et al.* [1992], and j_{NO_2} is calculated by the radiative transfer model of *Ruggaber et al.* [1994]. The reactions of NO with HO_2 and ClO are omitted here, as they account for a negligible NO conversion to NO_2 for the conditions of the Falcon flight. Individual uncertainties for $[O_3]$, k, and j_{NO_2} are 10%, 40% and 30%, respectively. The measured NO_2/NO ratios have an uncertainty of 30%. Within combined uncertainties the measured and calculated steady state NO_2/NO ratios agree, indicating that primary NO emitted by aircraft had approached already the steady state NO_2/NO ratio in the measured plumes. The estimated times required to reach the steady state ratio for the conditions of the individual plumes are approximately given by 3 times the time constant of $1/(j_{NO_2} + k[O_3])$, i.e., 26 min for plume 1 and 8 min for plume 6. As shown in Figure 3 the smallest plume age (15 min) is calculated for a plume positioned near the observed peak 5. This time is comparable to the expected time necessary to reach the steady state ratio for this peak (17 min).

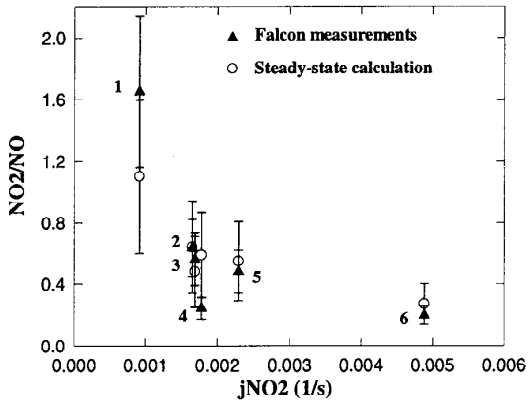

Figure 4. Comparison of measurements and steady state predictions for the NO_2/NO abundance ratios in exhaust plumes shown in Figure 2. NO_2/NO ratios are plotted versus calculated photodissociation coefficients.

The integrated CN abundances of plumes 2, 3, 5, and 6 are also listed in Table 1 together with the corresponding CN/NO_x ratios. The CN peaks of plumes 1 and 4 cannot be clearly distinguished from the background. For the considered plumes an average CN/NO_x ratio of 335 cm^{-3}ppbv^{-1} is obtained with a standard deviation of 70 cm^{-3}ppbv^{-1}. With the mean NO_x emission index of 16.5 g per 1 kg fuel (see below) for the source aircraft of the observed multiple plumes, a mean CN emission index of

$$EI[CN] = [CN]/[NO_x]\frac{EI[NO_x]M_{air}}{\rho_{air}M_{NO_2}} \approx 10^{16}\ \frac{\text{particles}}{\text{kg fuel}}$$

is obtained, where ρ_{air}, M_{air}, and M_{NO_2} denote the air density and molar masses of air and NO_2, respectively.

For comparison, one can estimate the emission index of soot (as total emitted particles per 1 kg fuel) by considering the typical range of soot emission indices for modern engines of $0.01 < EI[soot] < 0.1$ gkg^{-1}, $\rho_{soot} = 1.5$ gcm^{-3}, and assuming a mean diameter for soot particles of 30 nm. The obtained range for the soot emission index is $4.7\times10^{14} < EI[soot] < 4.7\times10^{15}$ particles per 1 kg fuel.

Consequently, the inferred particle emission index from the measurements is about a factor of 2 to 20

higher than calculated soot emission indices. This indicates that a large fraction of the measured CN in the moderately aged plumes are not soot particles but most probably sulfuric acid aerosols formed in the early jet phase of the aircraft plumes. Earlier observations in the aged exhaust plume of the Concorde supersonic aircraft in the lower stratosphere revealed similar ratios of total CN to nonvolatile CN [*Fahey et al.*, 1995a]; however, the inferred values for the total CN emissions indices are a factor of about 2 to 7 higher.

For plume 6 a SO_2 signature was clearly detected. Peak integration gives an SO_2/NO_x abundance ratio of 0.13. This yields an SO_2 emission index of 3 $g\,kg^{-1}$ considering the mean EI[NO_x] of 16.5 $g\,kg^{-1}$ for the source air traffic. The obtained EI[SO_2] is close to the upper limit of the sulfur mass content allowed for standard aviation kerosene of 0.3% by mass (corresponding to 6 g SO_2 per 1 kg fuel). The actual sulfur mass content varies strongly depending on the source refinery, with average values of 0.05% by mass [*Schumann*, 1996]. Considering this value, the mean EI[NO_x] of 16.5 $g\,kg^{-1}$, and the observed NO_x peak concentrations of 1 to 2 ppbv, an expected SO_2 enhancement of 40 to 80 pptv is calculated for the major NO_x plume signatures. Such SO_2 increases are hardly distinguishable from the observed variations of the SO_2 background concentrations in the 12-s SO_2 data of about 100 pptv.

Enhancements of the HNO_3 concentrations were not detectable for the major plumes 1 to 6. Considering the variations in the high-resolution (12 s) HNO_3 data of about 50 pptv with respect to 1-min mean values as an upper limit for HNO_3 formed in the plumes, less than about 10% of the NO_2 in the plumes has been oxidized to HNO_3 during the plume dispersion time span of 0.5 to 3 hs for the measuring conditions in accordance with model simulations of *Karol and Ozolin* [1994]. This observation is also in accordance with earlier measurements of the NO_y speciation in plumes of subsonic [*Arnold et al.*, 1992; *Zheng et al.*, 1994; *Fahey et al.*, 1995b] and supersonic [*Fahey et al.*, 1995a] aircraft which indicates that the HNO_3 fraction is small ($\leq$ 10% of NO_y) in exhaust plumes a few minutes after emission.

4. Comparison With Plume Model

In order to compare the measured NO_x increases along the corridor measuring legs with expected NO_x enhancements due to the spreading exhaust plumes of the observed air traffic in the investigation area, we have performed numerical simulations using a Gaussian plume model. Because of the uncertainty in the predicted plume positions along the Falcon track (about $\pm$ 0.25°), the measured fine structure of the multiple peaks cannot be described with the plume model. However, useful comparisons can be made between suitable integrated measuring data and model results of the NO_x distribution. An appropriate integration of the measured NO and NO_c signals also allows derivation of NO_x concentrations from the measurements for comparison with the model, which treats NO_x as a passive tracer.

4.1. Model Description

The Gaussian plume model used has been described in detail by *Konopka* [1995] and *Schumann et al.* [1995]. Briefly, the abundances of various exhaust species in the plume of a single airliner are represented by analytical solutions of the atmospheric diffusion equation. These solutions are Gaussian functions which are valid for spatially linear wind profiles, spatially constant diffusivities, and linear chemical reactions. In addition, all parameters of this model can depend step wisely on time. The concentration fields in the corridor result from linear superposition of such solutions for a multitude of plumes with different ages, source strengths, and spatial origins according to the distribution of the traffic.

With this approach, the NO_x concentration ρ_f along the Falcon track **f** for a single plume is written as

$$\rho_f(y,t) = A(t)\varphi(y,0,\hat{\sigma}_f(t))\,, \tag{2}$$

with

$$A(t) := \frac{c}{\sin\gamma}\varphi(h,0,\hat{\sigma}_v(t))\,, \tag{3}$$

$$\sigma_f^2(t) := \hat{\sigma}_f(t) := \frac{\hat{\sigma}_v(t)\hat{\sigma}_h(t) - \hat{\sigma}_s^2(t)}{\hat{\sigma}_v(t)\sin^2\gamma} \tag{4}$$

and the one-dimensional Gaussian function φ defined by

$$\varphi(x,\bar{x},\sigma) = (2\pi\sigma^2)^{-1/2}\exp\left[-\frac{(x-\bar{x})^2}{2\sigma^2}\right] \tag{5}$$

where $\bar{x}$ and σ denote the centroid and the standard deviation of φ. Here y is the horizontal space coordinate along the track of the Falcon relative to the plume centroid, and t is the effective plume age (i.e., relative to the beginning of the diffusion regime). The quantities A and σ_f give the integrated concentration and the standard deviation of the concentration peak profile ρ_f, respectively. Furthermore, γ denotes the angle, h is the distance between the main axis of the plume and the Falcon track, and c is the total mass of emitted NO_x per unit length along the flight path (in kilogram per meter).

The time-dependent functions $\hat{\sigma}_v$, $\hat{\sigma}_h$ and $\hat{\sigma}_s$ describe the (Gaussian) dynamics of the plume, and under some assumptions, these quantities can be expressed in terms of the atmospheric parameters [*Konopka*, 1995]. For this study we proceeded in the following way: First, the plume dispersion phase was divided into N steps $t_0 < t_1 < \ldots < t_N = t$ in which all parameters of dispersion are approximately constant. In particular, we assumed that during each time step $i = 1,\ldots,N$, the plume gets distorted by the wind shear s_i perpendicular to the plume axis and turbulent diffusion with an anisotropic, positive definite diffusivity tensor in terms

of horizontal, vertical, and skewed components D_{h_i}, D_{v_i}, and D_{s_i} with

$$D_{h_i}, D_{v_i} > 0\,, \qquad D_{s_i}^2 < D_{h_i} D_{v_i}\,. \tag{6}$$

After $N+1$ steps of dispersion, the functions $\hat{\sigma}_v$, $\hat{\sigma}_h$ and $\hat{\sigma}_s$ are given recursively by

$$\begin{aligned} \hat{\sigma}_h(t) &= \sigma_h^2(t) = \sigma_{h_N}^2, \quad \hat{\sigma}_s(t) = \hat{\sigma}_{s_N}, \\ \hat{\sigma}_v(t) &= \sigma_v^2(t) = \sigma_{v_N}^2, \end{aligned} \tag{7}$$

with

$$\begin{aligned} \sigma_{h_{i+1}}^2 &= \frac{2}{3} s_i^2 D_{v_i} \Delta t^3 + (2 s_i D_{s_i} + s_i^2 \sigma_{v_i}^2) \Delta t^2 + \\ &\quad 2(s_i \hat{\sigma}_{s_i} + D_{h_i}) \Delta t + \sigma_{h_i}^2\,, \\ \hat{\sigma}_{s_{i+1}} &= s_i D_{v_i} \Delta t^2 + (s_i \sigma_{v_i}^2 + 2 D_{s_i}) \Delta t + \hat{\sigma}_{s_i}\,, \quad (8) \\ \sigma_{v_{i+1}}^2 &= 2 D_{v_i} \Delta t + \sigma_{v_i}^2\,, \quad (9) \end{aligned}$$

where

$$\Delta t := t_{i+1} - t_i, \qquad i = 1, \ldots, N-1,$$

and σ_{h_0} and σ_{v_0} are horizontal and vertical standard deviations at the beginning of the dispersion regime, respectively. Furthermore, we assumed $\hat{\sigma}_{s_0} = 0$.

4.2. Input Parameters

The model requires various input parameters, some of which are only known with a considerable uncertainty. Simulations were done with a reference set of most likely input parameters and, in addition, for several sets of input parameters covering the ranges given in Table 2. The most important input parameters include the diffusion coefficients D_v and D_s, the vertical wind shear, and the effective emission height of the plumes relative to the source aircraft.

The Brunt-Väisälä frequency N and the vertical shear S of the total wind speed were obtained from the wind and temperature profiles measured during ascents and descents of the Falcon in the altitude range between 10.8 and 11.8 km before and after the horizontal corridor legs.

The diffusion coefficients D_v and D_h are determined from *Dürbeck and Gerz* [1995]. Due to weak vertical mixing in the upper troposphere, the vertical width of the plumes does not exceed about 200 m after 10 hours. Since the distance between two successive flight levels amounts to 600 m, the interaction between exhaust plumes released at different flight levels can be neglected for the timescales of several hours considered here. Consequently, only exhaust plumes emitted by the air traffic cruising at the Falcon measuring flight level of 37,000 feet as recorded from the radar screen have to be included in the simulations. The four aircraft passing the Falcon track prior to the period observed by radar are not considered (see Figure 1).

The source strength of NO_x depends on the fuel consumption c_f (in kilograms per second) of the individual aircraft-engine combination, the aircraft's ground speed v_g (in meters per second), and on the emission index of NO_x for the actual cruising conditions. For the aircraft considered, the mean emission index amounts to 16.5 g NO_x per 1 kg fuel (F. Deidewig, personal communication, 1995). The fuel consumptions at the cruising altitudes for the relevant aircraft were obtained from *Taylor* [1976] and vary between 2.8 (B-747) and 1.4 (EA-31) $\mathrm{kg\,s^{-1}}$. The mean ground speed amounts to 240 $\mathrm{m\,s^{-1}}$. The source strength c is given by

$$c := \frac{c_f EI[\mathrm{NO}_x]}{v_g}. \tag{10}$$

The Gaussian plume model is applied for the dispersion regime of the plumes, i.e., after the jet and vortex phase. For a wide-bodied aircraft the vortex phase ends after about 3 to 5 min. The corresponding vertical and horizontal plume widths σ_{v_0} and σ_{h_0} amount to 50 and 120 m, respectively [*Schumann et al.*, 1995]. The positions of the plume centroids along the Falcon legs and the plume ages were taken from the calculations shown in Figure 3. In addition, we supposed that the vertical deviation h of the plume centroid from the source traffic flight level (37,000 feet) at the beginning of the diffusion regime is given by half the maximum vertical displacement of the trailing vortex pair for the given stratification, i.e., $h = w_s/2N$, where w_s is the initial downward velocity of the vortex pair. For a typical value $w_s = 2\ \mathrm{m\,s^{-1}}$, one obtains $h = 45$ m.

Table 2. Input Parameters of the Gaussian Plume Model

Input Parameter	Reference Values	Range of Sensitivity Studies
Brunt-Väisälä frequency, N, $\mathrm{s^{-1}}$	0.022	
Vertical diffusivity, D_v, $\mathrm{m^2 s^{-1}}$		
$t < 13$ min	0.4	
$t > 13$ min	0.15	$0 < D_v < 0.6$
Horizontal diffusivity, D_h, $\mathrm{m^2 s^{-1}}$	20.0	
Skewed diffusivity, D_s, $\mathrm{m^2 s^{-1}}$	$0.5(D_v D_h)^{1/2}$	
Vertical wind shear $\lvert s \rvert$	0.005	$0 < \lvert s \rvert < 0.015$
$\perp$ to plume direction, $\mathrm{s^{-1}}$		
Vertical plume position h relative to source aircraft, m	45	$30 < h < 70$

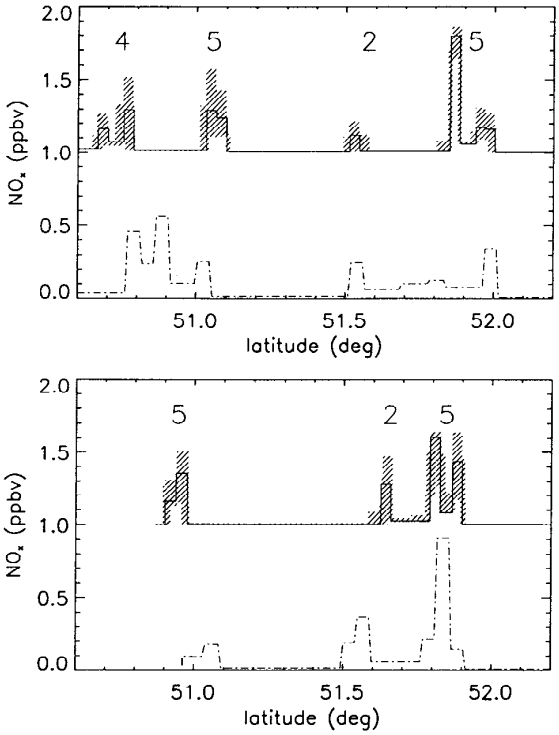

Figure 5. Comparison of observed NO_x plumes (dot-dashed lines) with simulations using a Gaussian plume model, for legs (top) B and (bottom) C. The solid lines show the calculated NO_x plumes with a reference set of input parameters. The dashed regions give the range obtained with the sensitivity studies (model results are shifted upward by 1 ppbv). The numbers give the total number of aircraft which cause the multiple plumes. Uncertainty in calculated positions of the plume structures is 0.25°. The simulated NO_x distribution was averaged in the same way as the experimental data.

4.3. Comparison of Multiple Plumes

Figure 5 presents the simulated NO_x increases along the Falcon measuring legs B and C for the reference case (solid lines). Also shown is the calculated range of variability caused by the uncertainty of the input parameters (dashed regions). In addition, the number of source aircraft which are responsible for the various plume structures are given.

For comparison, the measured NO_x increases are also included in Figure 5. The resultant NO and NO_c peaks were averaged over time, with a time step equal to 20 s. Larger time steps were used when the integral values of NO_c were below 2 ppbv s to improve count statistics. Finally, NO_x were determined from the average NO and NO_c.

Taking into account the uncertainties of the model input parameters, the simulated and measured NO_x plume peak concentrations and their positions along the Falcon track correspond fairly well. The simulations show that the measured NO_x structures can be attributed to multiple exhaust plumes caused by a superposition of 2 to 5 individual plumes with ages between about 15 min and 3 hours.

4.4. Plume Mixing Lifetime

From the Gaussian plume model one may estimate the typical mixing timescale, defined as the time after which the maximum concentration of NO_x in an exhaust plume caused by a single aircraft becomes comparable with typical variations of NO_x background concentrations. $[NO_x]_{max}$ is obtained from equations (2) to (4), i.e.,

$$[NO_x]_{max} = \frac{cM_{air}}{2\pi\rho_{air}M_{NO_2}\sqrt{\Delta(t)}} \tag{11}$$

with

$$s\Delta(t) = \hat{\sigma_h}(t)\hat{\sigma_v}(t) - \hat{\sigma_s}(t)^2, \tag{12}$$

s where $\sigma_h(t)$, $\sigma_v(t)$, and $\sigma_s(t)$ are given through relations (7) and (8). For a typical aircraft with EI[NO_x] = 16.5 gkg^{-1} and c_f = 2.65 kgs^{-1}, the calculated decrease of the NO_x peak concentration in the spreading plume for reference parameters given in Table 2 is shown in Figure 6 for different values of s.

After about 5 to 10 hs, the peak NO_x concentration in the plume is reduced to about 50 pptv, i.e., to a value comparable to variations of NO_x background abundances in the upper troposphere. The related vertical and horizontal width of the plume amounts to about 200 m and 20 km, respectively. Note that the mixing times determined here should be regarded as upper limits, since horizontal gradients of the wind field which may enhance mixing were neglected in the model.

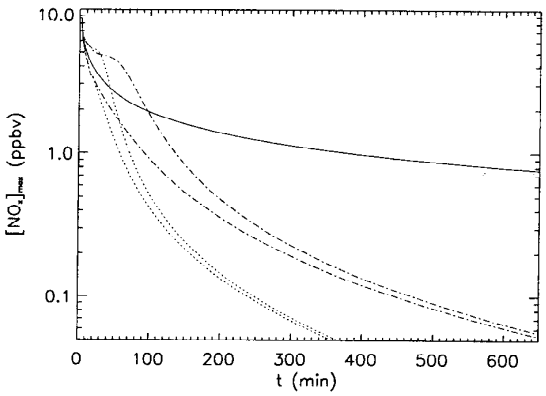

Figure 6. Peak plume values of NO_x versus plume age calculated from the Gaussian plume model for different values of s and D_s. The solid, dot-dashed, and dotted lines are calculated with s = 0, 0.005, and 0.015 s^{-1}, respectively. The upper and lower parts of the double lines correspond to $D_s = (D_v D_h)^{1/2}$ and $D_s = 0$.

5. Conclusions

Signatures of air traffic emissions have been detected in the North Atlantic flight corridor during peak traffic hours for NO, NO_2, SO_2 and particles by aircraft measurements across the main traffic routes. Peak concentrations in the exhaust plumes exceed background levels by factors of 30 (NO_x), 5 (SO_2), and 3 (CN) for the measuring conditions.

The source aircraft were identified from radar observations. The emissions measured at fixed flight level were caused by 22 wide-body aircraft which passed the measurement leg of 400 km length at 12°W within 5 hours during or before the measurement period. Calculations of predicted plume intersection points along the measuring tracks reveal that the measured concentration enhancements for NO_x, SO_2, and CN are mainly due to aircraft emissions in plumes with ages between 15 min and 3 hs. Hence the major observed peaks are due to superpositions of several relatively fresh plumes.

An analysis of the partitioning of NO and NO_2 in the observed peaks showed that primary emitted NO had approached already the steady state NO_2/NO ratios as expected for the determined plume ages. Observed CN/NO_x abundance ratios in the major plumes reveal a mean emission index of 10^{16} particles per 1 kg fuel burnt by the corridor traffic. A comparison with calculated EI for emitted soot indicates that the measured CN increases in the aged plumes are only to a smaller fraction due to soot particles. The measured mean CN/NO_x ratio of 300 $cm^{-3}ppbv^{-1}$ in aged plumes also indicates a mean CN increase in the North Atlantic flight corridor of about 30 cm^{-3} considering typical calculated large-scale NO_x increases by air traffic in this area of 100 pptv [e.g., *Brasseur et al.*, 1996]. This represents a marked perturbation of CN background concentrations of about 100 to 300 cm^{-3}.

The measured NO_x plume concentrations compare fairly well with NO_x enhancements computed with a Gaussian plume model if horizontal and vertical diffusivities are used as derived by large-eddy simulation [*Dürbeck and Gerz*, 1995] and measurements [*Schumann et al.*, 1995].

The simulated and measured distribution of NO_x in the corridor is very inhomogeneous. The spatial fraction of sections with enhanced concentrations (above 200 pptv in NO peaks) along cross-corridor tracks of about 400 km length is calculated to be 4% during heavy traffic conditions. About 30% of the total NO_x abundance is confined in plumes along the cross-corridor routes during traffic peak hours. It would be difficult to identify an aircraft contribution to the ambient NO_x abundance in the corridor region for observation times several hours after the major fraction of the corridor aircraft traffic has passed the investigation area for meteorological conditions where the exhaust plumes were strongly spread horizontally and vertically.

Hence studies of large scale signatures of air traffic emissions, i.e., at the scale of the corridor, should focus on synoptical situations favorable for accumulations of corridor traffic emissions, e.g., a stagnant anticyclone located in a major flight corridor. Such measurements have been performed recently during a second POLINAT campaign over the North Atlantic.

Appendix: Calculation of Plume Positions and Ages

We consider a measuring aircraft (Falcon) flying at constant altitude and an arbitrary airliner crossing the Falcon track at the same altitude. In a two-dimensional Cartesian approximation (see Figure 7), the Falcon and the airliner tracks can be described as two time-dependent straight lines $\mathbf{r}_f(t)$ and $\mathbf{r}_a(t)$. Here, the Falcon flies along the x_2 axis. Furthermore, we assume constant, two-dimensional velocities of the Falcon $[0, u_{2f}]$, the airliner $[u_{a1}, u_{a2}]$, and the wind $[u_{w1}, u_{w2}]$, respectively. The vertical component of the wind is neglected. The plume position $\mathbf{r}_p$ at time t for a plume released at time t_0 is given by

$$\mathbf{r}_p(t, t_0) = \begin{cases} x_{p1}(t, t_0) = x_{a1}(t_0) + u_{w1}(t - t_0) \\ x_{p2}(t, t_0) = x_{a2}(t_0) + u_{w2}(t - t_0) \end{cases} \quad (13)$$

where $\mathbf{r}_a := [x_{a1}, x_{a2}]$ with

$$\mathbf{r}_a(t) = \begin{cases} x_{a1}(t) = x_{a1r} + u_{a1}(t - t_{ar}) \\ x_{a2}(t) = x_{a2r} + u_{a2}(t - t_{ar}) \end{cases} \quad (14)$$

is the track of the airliner. Here, $[x_{a1r}, x_{a2r}]$ is the position of the airliner at the reference time t_{ar}. The Falcon path is described through

$$\mathbf{r}_f(t) = \begin{cases} x_{f1}(t) = 0 \\ x_{f2}(t) = x_{f2r} + u_{f2}(t - t_{fr}) \end{cases} \quad (15)$$

where $[0, x_{f2r}]$ is the Falcon position at $t = t_{fr}$. The cross condition between the plume and the Falcon track

$$\mathbf{r}_p(t_m, t_0) = \mathbf{r}_f(t_m) \quad (16)$$

determines the release and the cross times t_0 and t_m, respectively. The solution of this linear system of equations can be written in the following form:

$$t_0 = (\det \mathbf{A})^{-1}(b_2 A_{11} - b_1 A_{21}), \quad (17)$$

$$t_m = (\det \mathbf{A})^{-1}(b_1 A_{22} - b_2 A_{12}) \quad (18)$$

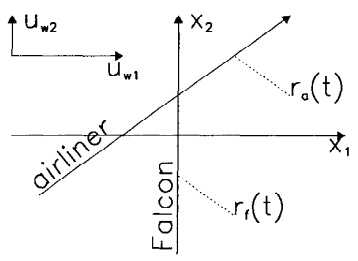

Figure 7. Sketch of the notation used.

with

$$\mathbf{A} = \begin{pmatrix} u_{w1} & u_{a1} - u_{w1} \\ u_{w2} - u_{f2} & u_{a2} - u_{w2} \end{pmatrix} \quad (19)$$

$$\mathbf{b} = \begin{pmatrix} -x_{a1r} + u_{a1} t_{ar} \\ x_{f2r} - x_{a2r} + u_{a2} t_{ar} - u_{f2} t_{fr} \end{pmatrix} \quad (20)$$

The plume age is given by $t_{age} = t_m - t_0$.

Acknowledgments. We are grateful for the contributions of the Falcon pilots, F. Rösler, R. Welser, and C. Feigl, and R. Marquardt of DLR; G. Kirchner of MPI-K; A.R. Hopkins, and J.D. Paladino of UMR; and H. Ovarlez and E. Landais of LMD in acquiring this data set. We also express our appreciation to the personnel of the Air Traffic Control Centre of Shannon for their expert support of the flight operations, Shanwick Oceanic Air Traffic Control in Prestwick for providing air traffic data, and P. van Velthoven of the Royal Netherlands Meteorological Institute (KNMI) for meteorological forecasts. We thank F. Deidewig of Institut für Antriebstechnik, DLR, for calculating the No_x emission indices for the corridor air traffic. This research was supported by the Commission of the European Union within the POLINAT project and by the German Bundesministerium für Bildung, Wissenschaft, Forschung und Technologie (BMBF) within the project "Schadstoffe in der Luftfahrt."

References

Arnold, F., and G. Hauck, Lower stratosphere trace gas detection using active chemical ionization mass spectrometry, *Nature*, *315*, 307–309, 1985.

Arnold, F., and G. Knop, Stratospheric trace gas detection using a new balloon-borne acims method, *Int. J. Mass Ion Process.*, *81*, 33–44, 1987.

Arnold, F., J. Scheid, T. Stilp, H. Schlager, and M. E. Reinhardt, Measurements of jet aircraft emissions at cruise altitude, I; The odd-nitrogen gases NO, NO_2, HNO_2 and HNO_3, *Geophys. Res. Lett.*, *19*, 2421–2424, 1992.

Atkinson, R., D. L. Baulch, R. A. Cox, R. F. Hampson Jr., J. A. Kerr, and J. Troe, Evaluated kinetic and photochemical data for atmospheric chemistry: Supplement IV, *Atmos. Environ., Part A*, *26*, 1187–1230, 1992.

Beck, J. P., C. E. Reeves, A. A. M. de Leeuw, and S. A. Penkett, The effects of aircraft emissions on tropospheric ozone in the northern hemisphere, *Atmos. Environ., Part A*, *26*, 17–29, 1992.

Bögel, W., and R. Baumann, Test and calibration of the DLR Falcon wind measuring system by maneuvers, *J. Atmos. Oceanic Technol.*, *8*, 5–18, 1991.

Brasseur, G. P., J. F. Müller, and C. Granier, Atmospheric impact of NO_x emissions by subsonic aircraft: A three-dimensional model study, *J. Geophys. Res.*, *101*, 1423–1428, 1996.

Dürbeck, T., and T. Gerz, Large-eddy simulation of aircraft exhaust plumes in the free atmosphere: Effective diffusivities and cross-sections, *Geophys. Res. Lett.*, *22*, 3203–3206, 1995.

Ehhalt, D. H., and F. Rohrer, The impact of commercial aircraft on tropospheric ozone, in *The Chemistry of the Atmosphere-Oxidants and Oxidation in the Earth Atmosphere, 7th BOC Pristley Conference, Lewisburg, Pennsylvania, 1994*, edited by A. Bandy, pp. 105–120., Royal Soc. of Chem., London, 1995.

Fahey, D. W., et al., Emission measurements of the Concorde supersonic aircraft in the lower stratosphere, *Science*, *270*, 70–74, 1995a.

Fahey, D. W., et al., In situ observations in aircraft exhaust plumes in the lower stratosphere at mid latitudes, *J. Geophys. Res.*, *100*, 3065–3074, 1995b.

Fontijin, A., A. J. Sabadell, and R. Ronco, Homogeneous chemiluminecence measurement of nitric oxide with ozone, *Anal. Chem.*, *42*, 575–579, 1970.

Frenzel, A., and F. Arnold, Sulfuric acid cluster ion formation by jet engines: Implications for sulfuric acid formation and nucleation, in *Impact of Emissions From Aircraft and Spacecraft Upon the Atmosphere. Proceedings of an International Scientific Colloquium, Köln (Cologne), Germany, April 18–20*, edited by U. Schumann and D. Wurzel, Deutsche Forschungsanstalt für Luft- und Raumfahrt-Mitt., 94-06, 106–112, 1994.

Hagen, D. E., P. D. Whitefield, M. B. Trueblood, and H. V. Lilenfeld, Particles and aerosols characterized in real time from harsh environments using the UMR mobile aerosol sampling system (MASS), AIAA Pap. 93-2344, 1993.

Johnson, C., J. Henshaw, and G. McInnes, Impact of aircraft and surface emissions of nitrogen oxides on tropospheric ozone and global warming, *Nature*, *355*, 69–71, 1992.

Kärcher, B., T. Peter, and R. Ottmann, Contrail formation: Homogeneous nucleation of H_2SO_4/H_2O droplets, *Geophys. Res. Lett.*, *22*, 1501–1504, 1995.

Karol, I. L., and Y. E. Ozolin, Small- and medium-scale effects on high-flying aircraft exhausts on the atmospheric composition, *Ann. Geophys.*, *12*, 979–985, 1994.

Kley, D., and M. McFarland, Chemiluminescence detector for NO and NO_2, *Atmos. Technol.*, *12*, 63–69, 1980.

Konopka, P., Analytical Gaussian solutions for anisotropic diffusion in a linear shear flow, *J. Non-Equilib. Thermodyn.*, *20*, 78–91, 1995.

Miake-Lye, R. C., R. C. Brown, M. R. Anderson, and C. E. Kolb, Calculation of condensation and chemistry in an aircraft, in *Impact of Emissions From Aircraft and Spacecraft Upon the Atmosphere. Proceedings of an International Scientific Colloquium, Köln (Cologne), Germany, April 18–20*, edited by U. Schumann and D. Wurzel, Deutsche Forschungsanstalt für Luft- und Raumfahrt-Mitt., 94-06, 274–279, 1994.

Möhler, O., T. Reiner, and F. Arnold, A novel aircraft-based tandem mass spectrometer for atmospheric ion and trace gas measurements, *Rev. Sci. Instrum.*, *86*, 1763–1766, 1993.

Ovarlez, J., Stratospheric water vapor measurements in the tropical zone by means of a frost point hygrometer on board long-duration balloons, *J. Geophys. Res.*, *96*, 15,541–15,545, 1991.

Ovarlez, J., and H. Ovarlez, Stratospheric water vapor content evolution during EASOE, *Geophys. Res. Lett.*, *21*, 1235–1238, 1994.

Reiner, T., and F. Arnold, Laboratory flow reactor measurements of the reaction $SO_3+H_2O+M \rightarrow H_2SO_4+M$: Implications for gaseous H_2SO_4 and aerosols formation in the plumes of jet aircraft, *Geophys. Res. Lett.*, *20*, 2659–2662, 1993.

Reiner, T., and F. Arnold, Laboratory investigations of gaseous sulfuric acid via $SO_3+H_2O+M \rightarrow H_2SO_4+M$, measurement of the rate coefficients and product identification, *J. Chem. Phys.*, *101*, 7399–7407, 1994.

Ridley, B. A., and L. C. Howlett, An instrument for nitric oxide measurements in the stratosphere, *Rev. Sci. Instrum.*, *45*, 742–746, 1974.

Ruggaber, A., R. Plugi, and T. Nakajima, Modelling of radiation quantities and photolysis frequencies in the troposphere, *J. Atmos. Chem.*, *18*, 171–210, 1994.

Schlager, H., P. Schulte, H. Volkert, R. Busen, and U. Schumann, Observations of enhanced nitric oxide abundances within the North Atlantic flight corridor, in *Impact of Emissions From Aircraft and Spacecraft Upon the Atmosphere. Proceedings of an International Scientific Colloquium, Köln (Cologne), Germany, April 18–20*, edited by U. Schumann and D. Wurzel, Deutsche Forschungsanstalt für Luft- und Raumfahrt-Mitt., 94-06, 336–341, 1994.

Schulte, P., and H. Schlager, In-flight measurements of cruise altitude nitric oxide emission indices of commercial jet aircraft, *Geophys. Res. Lett.*, *23*, 165–168, 1996.

Schumann, U., On the effect of emissions from aircraft engines on the state of the atmosphere, *Ann. Geophys.*, *12*, 365–384, 1994.

Schumann, U., On conditions for contrail formation from aircraft exhausts, *Meteorol. Z.*, *5*, 4–23, 1996.

Schumann, U., and P. Konopka, A simple estimate of the concentration field in a flight corridor, in *Impact of Emissions From Aircraft and Spacecraft Upon the Atmosphere. Proceedings of an International Scientific Colloquium, Köln (Cologne), Germany, April 18–20*, edited by U. Schumann and D. Wurzel, Deutsche Forschungsanstalt für Luft- und Raumfahrt-Mitt., 94-06, 354–359, 1994.

Schumann, U., P. Konopka, R. Baumann, R. Busen, T. Gerz, H. Schlager, P. Schulte, and H. Volkert, Estimation of diffusion parameters of aircraft exhaust plumes near the tropopause from nitric oxide and turbulence measurements, *J. Geophys. Res.*, *100*, 14,147–14,162, 1995.

Schumann, U., J. Ström, R. Busen, R. Baumann, K. Gierens, M. Krautstrunk, F. S. Schröder, and J. Stingl, In situ observations of particles in jet aircraft exhausts and contrails for different sulfur containing fuel, *J. Geophys. Res.*, *101*, 6853–6869, 1996.

Taylor, J. W. R. (ed.), *Jane's All the World's Aircraft 1975–76*,. Jane's Yearbooks, London, 1976.

Whitefield, P. D., and D. E. Hagen, Particulate and aerosol sampling from angular sector combustor rigs using the UMR mobile aerosol sampling system, AIAA Pap. 95-0111, 1995.

Whitefield, P. D., D. E. Hagen, and H. Schlager, Particulate emissions in the exhaust plume from commercial jet aircraft under cruise conditions, *J. Geophys. Res.*, *101*, 19,551–19,557, 1996.

Wilson, J. C., V. T. Lai, and S. D. Smith, Measurements of condensation nuclei above the jet stream: Evidence for cross jet transport by waves and new particle formation at high altitudes, *J. Geophys. Res.*, *96*, 17415–17423, 1991.

World Meteorological Organization, (WMO), Scientific assessment of ozone depletion: 1994, Rep. 37, Global Ozone Res. and Monit. Proj., Geneva, 1995.

Zhao, J., and R. P. Turco, Nucleation simulations in the wake of a jet aircraft in stratospheric flight, *J. Aerosol Sci.*, *26*, 779–795, 1995.

Zheng, J., A. J. Weinheimer, B. A. Ridley, S. C. Liu, G. W. Sachse, B. E. Anderson, and J. E. Collins Jr., An analysis of aircraft exhaust plumes from accidental encounters, *Geophys. Res. Lett.*, *21*, 2579–2582, 1994.

F. Arnold and M. Klemm, Bereich Atmosphärenphysik, Max-Planck-Institut für Kernphysik, Postfach 10 39 80, D-69029 Heidelberg, Germany (e-mail: Schneid@kosmo.mpi-hd.mpg.de Klemm@kosmo.mpi-hd.mpg.de)

D. E. Hagen and P. D. Whitefield, Laboratory for Cloud and Aerosol Science, University of Missouri-Rolla, Rolla, MO 65401 (e-mail: Hagen@umrvmb.umr.edu, whitefie@umrvmb.umr.edu)

P. Konopka, H. Schlager, P. Schulte, U. Schumann, and H. Ziereis, Institut für Physik der Atmosphäre, Deutsche Forschungsanstalt für Luft- und Raumfahrt Oberpfaffenhofen, D-82234 Weßling, Germany (e-mail: Paul.Konopka@dlr.de, Hans.Schlager@dlr.de, Peter.Schulte@dlr.de, Ulrich.Schumann@dlr.de Helmut.Ziereis@dlr.de)

J. Ovarlez, Laboratoire de Météorologie Dynamique du CNRS, Ecole Polytechnique, F-91128 Palaieau, France (e-mail: ovarlez@LMDX04.polytechnique.fr)

(Received July 10, 1996; revised November 14, 1996; accepted November 14, 1996.)